Accelerate stochastic calculation of random-phase approximation correlation energy difference with an atom-based correlated sampling

Yu-Chieh Chi

Department of Scientific Computing,

Florida State University, Tallahassee, Florida 32306, USA

Chen Huang*

Department of Scientific Computing,

Materials Science and Engineering Program,

and National High Magnetic Field Laboratory,

Florida State University, Tallahassee, Florida 32306, USA

(Dated: January 12, 2021)

Abstract

A kernel polynomial method (KPM) is developed to calculate the random phase approximation (RPA) correlation energy. In the method, the RPA correlation energy is formulated in terms of the matrix that is the product of the Coulomb potential and the density linear response functions. The integration over the matrix's eigenvalues is calculated by expanding the density of states of the matrix in terms of the Chebyshev polynomials. The coefficients in the expansion are obtained through stochastic sampling. Since it is often the energy difference between two systems that is of much interest in practice, another focus of this work is to develop a correlated sampling scheme to accelerate the convergence of the stochastic calculations of the RPA correlation energy difference between two similar systems. The scheme is termed the atom-based correlated sampling (ACS). The performance of ACS is examined by calculating the isomerization energy of acetone to 2-propenol and the energy of the water-gas shift reaction. Using ACS, the convergences of these two examples are accelerated by 3.6 and 4.5 times, respectively. The methods developed in this work are expected to be useful for calculating RPA-level reaction energies for the reactions that take place in local regions, such as calculating the adsorption energies of molecules on transition metal surfaces for modeling surface catalysis.

I. INTRODUCTION

Kohn-Sham density functional theory (KS-DFT)[1,2] is widely used for calculating the properties of molecules and materials. Its accuracy is determined by the approximation used for the exchange-correlation (XC) functional. Local density approximation and generalized gradient approximation suffer from the self-interaction error.[3,4] Hybrid functionals partially resolve the self-interaction error by containing a fraction of the exact exchange (EXX).[5] To go beyond hybrid functional, one can combine EXX with a compatible correlation energy functional. The random phase approximation (RPA) correlation energy[6–13], derived based on the adiabatic connection fluctuation and dissipation theorem,[6–9] is a good candidate, since the RPA correlation largely screens the long-range exchange interaction in metallic systems. This makes EXX+RPA applicable to both metallic and non-metallic systems. DFT calculations based on EXX+RPA have been shown to give reasonable predictions to many challenging problems, such as the α-γ phase transition of cerium[14] and the CO adsorption on transition metals.[15]

One obstacle in the widespread use of the RPA correlation energy is its high computational cost and steep computational scaling. Conventional implementations of the RPA correlation energy scale as $\mathcal{O}(N^4)$,[13,16–19] where N denotes the number of electrons. Recently, cubic-scaling implementations based on Green's function[20] and Gaussian basis functions[21] were demonstrated. To further reduce the computational scaling, Kálly developed a linear-scaling RPA method[22] based on the cluster-in-molecule method[23]. Ochsenfeld and coworkers also developed a linear-scaling RPA method by formulating the RPA correlation energy in terms of the atomic orbitals through a double-Laplace transformation.[24,25] These linear-scaling methods are suitable for calculating the relative energy between two systems that only differ much in a local region. In this work, we also focus on calculating the relative energy between two similar systems.

Different from aforementioned deterministic approaches, Neuhauser and coworkers developed a stochastic approach to calculate the RPA correlation energy.[26] The cost of their method scales linearly with the system's size for achieving a fixed error in total energy per electron. One advantage of stochastic methods is that one can stop the stochastic sampling whenever the sampling error drops below a given threshold. This make stochastic methods suitable for calculating the energy difference between two systems that only differ much

in the region of interest. By performing the correlated sampling, the error does not grow with the system's size but is determined by the size of the region of interest.[26] We note that stochastic methods have also been developed for other electronic structure calculations, such as the GW method,[27] KS-DFT,[28] the Bethe-Salpeter equation,[29] time-dependent DFT,[30] the second-order Møller-Plesset perturbation theory,[31] and the Hartree-Fock exchange.[32]

In this work, we develop a new stochastic method for calculating the RPA correlation energy. The method is formulated based on the kernel polynomial method (KPM)[33–37] and is termed RPA-KPM. Our method is different from Ref.[26] by how the RPA correlation is formulated. In our method, the RPA correlation energy is written in terms of the eigenvalues $\{x_i\}$ of the matrix $v_c^{1/2}\chi_0(iu)v_c^{1/2}$, where $\chi_0(iu)$ is the KS linear response at the imaginary frequency iu and $v_c(\mathbf{r},\mathbf{r}') = 1/|\mathbf{r}-\mathbf{r}'|$ is the Coulomb potential. The density of states (DOS) for the eigenvalues is then stochastically evaluated using KPM. As demonstrated in this work, the absolute RPA correlation energies converge slowly with respect to the number of samplings. Instead, in this work we focus on computing the RPA energy difference between two similar systems that only differ much in the region of interest. Such scenarios are often encountered in practice when reactions take place in a local region. Since RPA correlation is more accurate for isogyric processes, our stochastic RPA method is recommended for studying isogyric processes.

Correlated sampling is a common technique for accelerating the convergence of sampling. For the case that the atoms from two systems have similar coordinates, a correlated sampling can be performed to accelerate the convergence of energy-difference calculations, by employing the same sequence of random numbers for computing the two systems' RPA correlation energies.[26] However, in the region of interest the atoms from the two systems can have very different coordinates due to the chemical reaction, and therefore the correlated sampling cannot be performed. One goal of this work is to develop a method to accelerate the RPA energy difference calculations by *partially* restoring the correlation sampling. The method is termed the atom-based correlated sampling (ACS). With ACS, a system is roughly divided into two regions: (a) the atomic regions near nuclei and (b) the bond regions. With ACS, the samplings in the atomic regions between two systems are correlated, which effectively reduces the sampling error. The implementation of ACS is simple and only requires additional RPA-KPM calculations on atoms. Compared to RPA-KPM calculations on entire systems, the cost of ACS becomes negligible for large systems.

The paper is organized as follows. We first formulate the RPA correlation energy in the framework of KPM. We then discuss the ACS scheme. The performance of RPA-KPM with and without using ACS is examined by calculating the RPA correlation energy difference for two cases: (a) the isomerization of acetone to 2-propenol and (b) the energy of the water-gas shift reaction. For both cases, convergence is much accelerated by ACS. ACS is then examined in detail with a H_8 chain. In the end, the computational cost of RPA-KPM, ACS, and the stochastic method developed in Ref.[26] are analyzed.

II. THEORETICAL METHODS

A. RPA correlation energy formulated in the framework of KPM

The RPA correlation energy is[7,9,38]

$$E_c^{\mathrm{RPA}} = \frac{1}{2\pi}\int_0^\infty du \mathrm{Tr}[\ln(1-\chi_0(\mathbf{r},\mathbf{r}';iu)v_c)+\chi_0(\mathbf{r},\mathbf{r}';iu)v_c], \tag{1}$$

where $v_c(\mathbf{r},\mathbf{r}') = 1/|\mathbf{r}-\mathbf{r}'|$ is the Coulomb potential. $\chi_0(\mathbf{r},\mathbf{r}';iu)$ is the KS linear response function at the imaginary frequency iu and can be explicitly expressed in term of KS orbitals ($\{\phi_j(\mathbf{r})\}$), eigenvalues ($\{\epsilon_j\}$), and occupation numbers ($\{f_j\}$) as

$$\chi_0(\mathbf{r},\mathbf{r}';iu) = 2\sum_j\sum_k (f_j-f_k)\frac{\phi_j^*(\mathbf{r})\phi_k(\mathbf{r})\phi_k^*(\mathbf{r}')\phi_j(\mathbf{r}')}{\epsilon_j-\epsilon_k+iu}, \tag{2}$$

where indices j and k loop over all the KS orbitals. Non-spin-polarized case is considered in this work. Tr[...] in Eq. 1 represents

$$\mathrm{Tr}[AB] = \int\int d\mathbf{r}d\mathbf{r}' A(\mathbf{r},\mathbf{r}')B(\mathbf{r},\mathbf{r}').$$

Due to the fact the trace is invariant under cyclic permutations, $\chi_0 v_c$ in Eq. 1 can be replaced by $v_c^{1/2}\chi_0 v_c^{1/2}$, which is denoted by M in this work, that is, $M(iu) = v_c^{1/2}\chi_0(iu)v_c^{1/2}$.

To formulate the RPA correlation energy using KPM, we write it in terms of the density of states (DOS), $\rho(x;u)$, for M's eigenvalues

$$E_c^{\mathrm{RPA}} = \frac{1}{2\pi}\int_0^\infty du \int_{x_{\min}}^0 \rho(x;u)[\ln(1-x)+x]dx, \tag{3}$$

where x is M's eigenvalue and $x_{\min}$ is the lowest eigenvalue. The upper limit of the integral is zero, since M is semi-negative definite. In order to expand $\rho(x;u)$ in terms of the Chebyshev

polynomials, we need to rescale M such that its eigenvalues are inside $(-1, 1)$, which is achieved with the linear transformation

$$\widetilde{M} = (M - b)/a, \tag{4}$$

with the scaling parameters a and b defined as

$$\begin{aligned} a &= (x_{\max} - x_{\min})/(2 - \delta) \\ b &= (x_{\max} + x_{\min})/2, \end{aligned} \tag{5}$$

where $x_{\max}$ and $x_{\min}$ are the maximum and minimum eigenvalues of M. In this work, $x_{\min}$ is calculated using the conjugate gradient method. $x_{\max}$ is set to zero. The parameter δ is a small positive number to make sure that all $\widetilde{M}$'s eigenvalues are inside (-1,1). δ is set to 0.01 in this work. The RPA correlation energy can then be written in terms of $\widetilde{M}$'s DOS as

$$E_c^{\mathrm{RPA}} = \int_0^\infty \frac{du}{2\pi} \int_{-1}^{1} \widetilde{\rho}(\widetilde{x}; u)[\ln(1 - (a\tilde{x} + b)) + a\tilde{x} + b]d\widetilde{x}, \tag{6}$$

where $\tilde{x}$ is the eigenvalue of $\widetilde{M}$. $\widetilde{\rho}$ is the DOS of $\widetilde{M}$ and is related to ρ as $\widetilde{\rho}(\widetilde{x}; u) = a\rho(x; u)$. $\widetilde{\rho}$ is expanded using the Chebyshev polynomials

$$\widetilde{\rho}(\widetilde{x}) = \frac{1}{\pi\sqrt{1 - \widetilde{x}^2}} \left[g_0\mu_0 + 2\sum_{n=1}^{N_m} g_n\mu_n T_n(\widetilde{x}) \right], \tag{7}$$

where $\{\mu_n\}$ are the moments given by

$$\mu_n = \mathrm{Tr}[T_n(\widetilde{M})]. \tag{8}$$

T_n is the n-th order Chebyshev polynomial. N_m is the number of moments for the expansion. $\{g_n\}$ are the Jackson kernels[39,40] for suppressing the Gibbs oscillations in the DOS:

$$g_n = \frac{(N_m - n + 1)\cos\frac{n\pi}{N_m+1} + \sin\frac{n\pi}{N_m+1}\cot\frac{\pi}{N_m+1}}{N_m + 1}. \tag{9}$$

Inserting Eq. 7 into Eq. 6, the RPA correlation energy becomes

$$E_c^{\mathrm{RPA}} = \frac{1}{2\pi} \int_0^\infty du \left[g_0c_0\mu_0 + 2\sum_{n=1}^{N_m} g_nc_n\mu_n \right], \tag{10}$$

where c_n is defined as

$$c_n = \int_{-1}^{1} \frac{1}{\pi\sqrt{1 - \widetilde{x}^2}} T_n(\widetilde{x})[\ln(1 - (a\widetilde{x} + b)) + (a\tilde{x} + b)]d\widetilde{x}. \tag{11}$$

Above integration is evaluated using the quadpack program.[41]

B. Stochastic calculation of moments

The key of KPM is to calculate the moments $\{\mu_n\}$. Due to the large size of $\widetilde{M}$, in Eq. 8 the trace is evaluated stochastically using the random vectors $\{|r\rangle\}$ as[33]

$$\mathrm{Tr}[T_n(\widetilde{M})] \approx \frac{1}{R}\sum_{r=1}^{R} \langle r|\, T_n(\widetilde{M})\, |r\rangle\,, \tag{12}$$

where R is the number of random vectors. Denote the i^{th} entry of $|r\rangle$ as ξ_{ri}. $\{\xi_{ri}\}$ is a random number and satisfy the conditions: $\langle\langle \xi_{rj}\rangle\rangle = 0$ and $\langle\langle \xi_{ri}\xi_{r'j}\rangle\rangle = \delta_{rr'}\delta_{ij}$, where $\langle\langle \cdots \rangle\rangle$ denotes the statistical average with respect to different realizations of random vectors. These conditions can be satisfied by setting ξ_{ri} to the normal random numbers with zero mean and unit variance. In this work, normal random numbers are generated using the Box-Muller scheme[42] in which uniform random numbers are generated using the RAN3 algorithm.[43]

Eq. 12 involves calculating the product of $T_n(\widetilde{M})$ and $|r\rangle$, which is calculated using the three-term recurrence relation of the Chebyshev polynomials

$$T_n(\widetilde{M})\,|r\rangle = 2\widetilde{M}T_{n-1}(\widetilde{M})\,|r\rangle - T_{n-2}(\widetilde{M})\,|r\rangle\,. \tag{13}$$

Above equation relies on calculating the product of $v_c^{1/2}\chi_0(iu)v_c^{1/2}$ and a vector. In this work, the product of $v_c^{1/2}$ and a vector is evaluated efficiently by transforming both $v_c^{1/2}$ and the vector to the Fourier space, since $v_c^{1/2}$ is diagonal in the Fourier space. The product of $\chi_0(iu)$ and a vector is calculated by solving the Sternheimer equation[44–46].

C. The atom-based correlated sampling

As demonstrated in later sections, the strength of RPA-KPM is to calculate the RPA energy difference between two similar systems that have the same composition. Denote the two systems as system 1 and system 2. Their RPA energy difference is

$$\Delta E_c^{\mathrm{RPA}} = E_{c1}^{\mathrm{RPA}} - E_{c2}^{\mathrm{RPA}}, \tag{14}$$

where E_{c1}^{RPA} and E_{c2}^{RPA} are the RPA correlation energies of the system 1 and the system 2, respectively. If the atoms in the two systems have similar coordinates, a correlated sampling can be performed by using the same sequence of random vectors to calculate E_{c1}^{RPA} and E_{c2}^{RPA}.

However, the correlated sampling cannot be performed, if the atoms in the two systems have completely different coordinates. To tackle this problem, in what follows we develop the ACS method. In ACS, additional RPA-KPM calculations are performed on each atom in both systems. To be specific, let's consider the atom i in the system 1. We remove all the atoms in the system 1 except the atom i. The atom i is kept at its original position. We then perform RPA-KPM calculation on this new system that only contains the atom i, employing the sequence of random vectors used for sampling the system 1. The atom i is set to neutral in the calculation, and the occupation numbers of its KS orbitals are assigned using the Fermi-Dirac smearing with a smearing temperature of 0.1 eV, which helps the KS-DFT calculations converge. Such RPA-KPM calculation is performed for all the atoms in the systems 1. Similarly, we perform RPA-KPM calculations on each atom in the system 2, using the same sequence of random vectors used for the system 2. We then calculate the RPA correlation contribution to the atomization energy (AE) as

$$E^{\mathrm{RPA}}_{\mathrm{AE},1} = E^{\mathrm{RPA}}_{c1} - \sum_{i=1}^{N_{\mathrm{atom}}} E^{\mathrm{RPA}}_{c1,\mathrm{atom}_i} \tag{15}$$

$$E^{\mathrm{RPA}}_{\mathrm{AE},2} = E^{\mathrm{RPA}}_{c2} - \sum_{i=1}^{N_{\mathrm{atom}}} E^{\mathrm{RPA}}_{c2,\mathrm{atom}_i}, \tag{16}$$

where i runs over all the atoms in each system and N_{atom} is the number of atoms. $E^{\mathrm{RPA}}_{c1,\mathrm{atom}_i}$ and $E^{\mathrm{RPA}}_{c2,\mathrm{atom}_i}$ are the atom i's RPA correlation energies calculated using RPA-KPM, as described above. The RPA correlation energy difference between the two systems is then calculated as

$$\Delta E^{\mathrm{RPA}}_{c,\mathrm{ACS}} = E^{\mathrm{RPA}}_{\mathrm{AE},1} - E^{\mathrm{RPA}}_{\mathrm{AE},2}. \tag{17}$$

$\Delta E^{\mathrm{RPA}}_{c,\mathrm{ACS}}$ defined in Eq. 17 converges faster than $\Delta E^{\mathrm{RPA}}_{c}$ defined in Eq. 14. The reason is that, by subtracting the atomic RPA correlation energies in Eqs. 15 and 16, we focus on calculating the bond energy difference between the two systems. In other words, the correlated sampling is achieved in the atomic regions, but not in the bond regions. To better understand ACS, let's consider a limiting case in which all the atoms in the two systems are well separated. For this case, $\Delta E^{\mathrm{RPA}}_{c}$ calculated using Eq. 17 is always zero, no matter how many random vectors are used.

D. The reduction of computational cost using ACS

The goal of ACS is to reduce the standard error from sampling $\Delta E_c^{\mathrm{RPA}}$, which in turn reduces the number of random vectors. Due to the central limit theorem, standard error decreases as $1/\sqrt{R}$, where R is the number of random vectors. The cost reduction (q) is then related to the standard error as

$$q = 1 - \left(\frac{\sigma_{\mathrm{err}}^{\mathrm{ACS}}}{\sigma_{\mathrm{err}}} \right)^2, \tag{18}$$

where $\sigma_{\mathrm{err}}^{\mathrm{ACS}}$ and σ_{err} are the standard errors for $\Delta E_{c,\mathrm{ACS}}^{\mathrm{RPA}}$ and $\Delta E_c^{\mathrm{RPA}}$, respectively. They are related to the variances as $\sigma_{\mathrm{err}}^{\mathrm{ACS}} = \frac{1}{R}\sqrt{\mathrm{Var}(\Delta E_{c,\mathrm{ACS}}^{\mathrm{RPA}})}$ and $\sigma_{\mathrm{err}} = \frac{1}{R}\sqrt{\mathrm{Var}(\Delta E_c^{\mathrm{RPA}})}$. In this work, E_{c1}^{RPA} and E_{c2}^{RPA} are calculated using two different sequences of random vectors for mimicking the case that the atoms in the two systems have completely different coordinates. Therefore, E_{c1}^{RPA} and E_{c2}^{RPA} are not correlated and we have

$$\mathrm{Var}(\Delta E_c^{\mathrm{RPA}}) = \mathrm{Var}(E_{c1}^{\mathrm{RPA}}) + \mathrm{Var}(E_{c2}^{\mathrm{RPA}}). \tag{19}$$

Similarly, the variance of $\Delta E_{c,\mathrm{ACS}}^{\mathrm{RPA}}$ is

$$\mathrm{Var}(\Delta E_{c,\mathrm{ACS}}^{\mathrm{RPA}}) = \mathrm{Var}(E_{\mathrm{AE},1}^{\mathrm{RPA}}) + \mathrm{Var}(E_{\mathrm{AE},2}^{\mathrm{RPA}}). \tag{20}$$

Eq. 18 then becomes

$$q = 1 - \frac{\mathrm{Var}(\Delta E_{c,\mathrm{ACS}}^{\mathrm{RPA}})}{\mathrm{Var}(\Delta E_c^{\mathrm{RPA}})}. \tag{21}$$

In the ideal case that $\mathrm{Var}(\Delta E_{c,\mathrm{ACS}}^{\mathrm{RPA}})$ is zero, we have $q = 1$, which means that the cost reduction is 100%. This only happens if all the atoms are well separated.

III. NUMERICAL DETAILS

The RPA-KPM method is implemented in the ABINIT program[47] (version 7.10.4). In Eq. 10, the integration over the frequency u is calculated using the Gauss–Legendre quadrature. The upper limit of the integral (u_{max}) is set to 10 a.u.. To have a high density of the Gauss–Legendre points in the low frequency region, the integration scheme in Ref.[48] is used. The integral $\int_0^{u_{\mathrm{max}}} f(u)du$ is first transformed to $\int_0^1 g(t)dt$ through the variable change $t = \exp(-(\alpha u)^{1/B})$ with $B = 2$. t is in the domain [0,1], and $g(t) = f(u(t))B(-\ln t)^{B-1}/(\alpha t)$. The upper limit u_{max} is related to α as $\alpha = (-\ln t)^B/u_{\mathrm{max}}$, and α is chosen such that u_{max} = 10.0 a.u.. The Gauss–Legendre quadrature on $\int_0^1 g(t)dt$ is performed for t with 16 nodes.

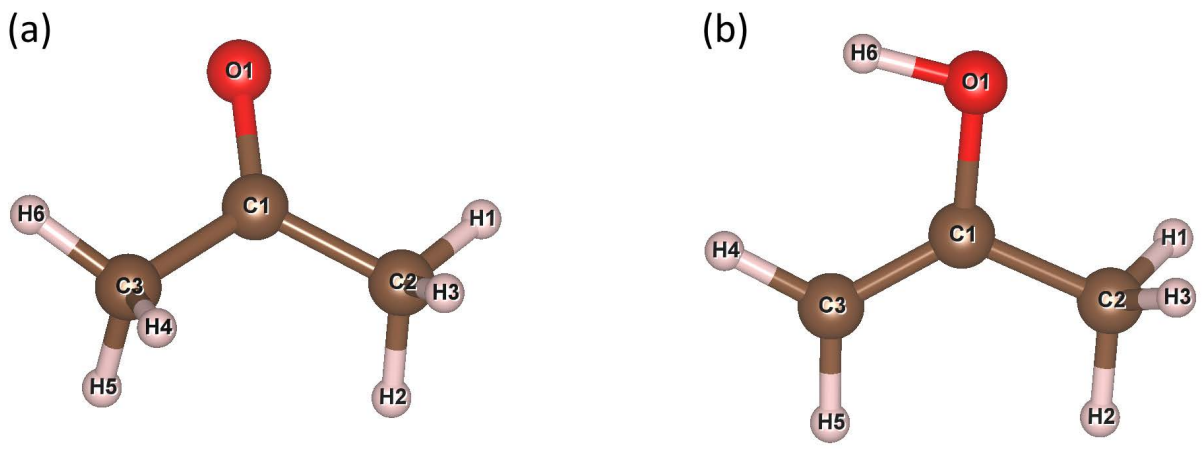

FIG. 1. Isomerization of (a) acetone to (b) 2-propenol by transferring H6. The oxygen, carbon, hydrogen atoms are red, brown, and grey, respectively. Figure is made using the VESTA program.[50]

IV. RESULTS AND DISCUSSIONS

The performance of RPA-KPM (with and without using ACS) is investigated with three examples: (1) the energy for the isomerization of acetone to 2-propenol (Fig. 1), (2) the energy of the water gas shift reaction, and (3) a H_8 chain. These systems are first calculated using the Perdew-Burke-Ernzerhof (PBE)[49] XC functional, based on which the RPA correlation energies are calculated using RPA-KPM. For all examples, two different sequences of random vectors are used for system 1 and system 2, to mimic the case that the atoms from the two systems have very different coordinates. The benchmarks are obtained by calculating the RPA correlation energies using the method developed in Ref.[46], that is, $\mathrm{Tr}\{\ln[1-\chi_0(iu)v_c]+\chi_0(iu)v_c\}$ is calculated as $\sum_{k=1}^{N_{\mathrm{eig}}}\ln(1-e_k)+e_k$, where $\{e_k\}$ are the eigenvalues of $v_c^{1/2}\chi_0(iu)v_c^{1/2}$ and N_{eig} is the number of eigenvalue values. $\Delta E_c^{\mathrm{RPA}}$ converges quickly with respect to N_{eig}. N_{eig} is 400 and 800 for the example 1 and the example 2, respectively. To save the computational cost, low kinetic energy cutoffs are used. Example 1, 2, and 3 are calculated using a kinetic energy cutoff of 200 eV, 400 eV, and 400 eV, respectively.

TABLE I. The lowest eigenvalues of $v_c^{1/2}\chi_0(iu)v_c^{1/2}$ for acetone, 2-propenol, hydrogen, carbon, and oxygen atoms, for the 16 frequencies. The lower limits $x_{\min}$ (Eq. 3) are also shown. Atomic units are used.

u	acetone	2-propenol	H	C	O	$x_{\min}$
1.03×10^{-5}	-3.077	-2.893	-0.469	-1.200	-1.049	-3.077
2.87×10^{-4}	-3.077	-2.893	-0.469	-1.200	-1.049	-3.077
1.76×10^{-3}	-3.077	-2.893	-0.469	-1.200	-1.049	-3.077
6.20×10^{-3}	-3.076	-2.891	-0.469	-1.200	-1.049	-3.076
1.64×10^{-2}	-3.067	-2.880	-0.468	-1.200	-1.048	-3.067
3.64×10^{-2}	-3.030	-2.832	-0.465	-1.191	-1.044	-3.030
7.21×10^{-2}	-2.907	-2.676	-0.452	-1.166	-1.030	-2.907
1.32×10^{-1}	-2.605	-2.338	-0.420	-1.094	-0.990	-2.605
2.29×10^{-1}	-2.116	-1.875	-0.356	-0.939	-0.902	-2.116
3.82×10^{-1}	-1.571	-1.439	-0.270	-0.703	-0.760	-1.571
6.21×10^{-1}	-1.074	-1.025	-0.186	-0.459	-0.590	-1.074
9.98×10^{-1}	-0.671	-0.656	-0.118	-0.308	-0.430	-0.671
1.61	-0.382	-0.378	-0.069	-0.190	-0.287	-0.382
2.66	-0.203	-0.204	-0.034	-0.104	-0.166	-0.203
4.68	-0.093	-0.093	-0.016	-0.047	-0.080	-0.093
10.0	-0.026	-0.026	-0.005	-0.013	-0.024	-0.026

A. Isomerization of acetone to 2-propenol

In this example, acetone is treated as the system 1 and 2-propenol is treated as the system 2. Table I lists the lowest eigenvalues of $v_c^{1/2}\chi_0(iu)v_c^{1/2}$ for all the 16 frequencies for acetone, 2-propenol, and each atom. For each frequency, $x_{\min}$ is set to the lowest eigenvalue and is used in all RPA-KPM calculations to achieve a good error cancellation for computing $\Delta E_c^{\mathrm{RPA}}$.

Fig. 2(a) shows that the convergence of E_c^{RPA} with respect to the number of moments is very slow. Fig. 2(b) shows $\Delta E_c^{\mathrm{RPA}}$ without using the ACS scheme, and a fast convergence is observed. With only 10 moments, $\Delta E_c^{\mathrm{RPA}}$ converges to within 0.01 eV. The results

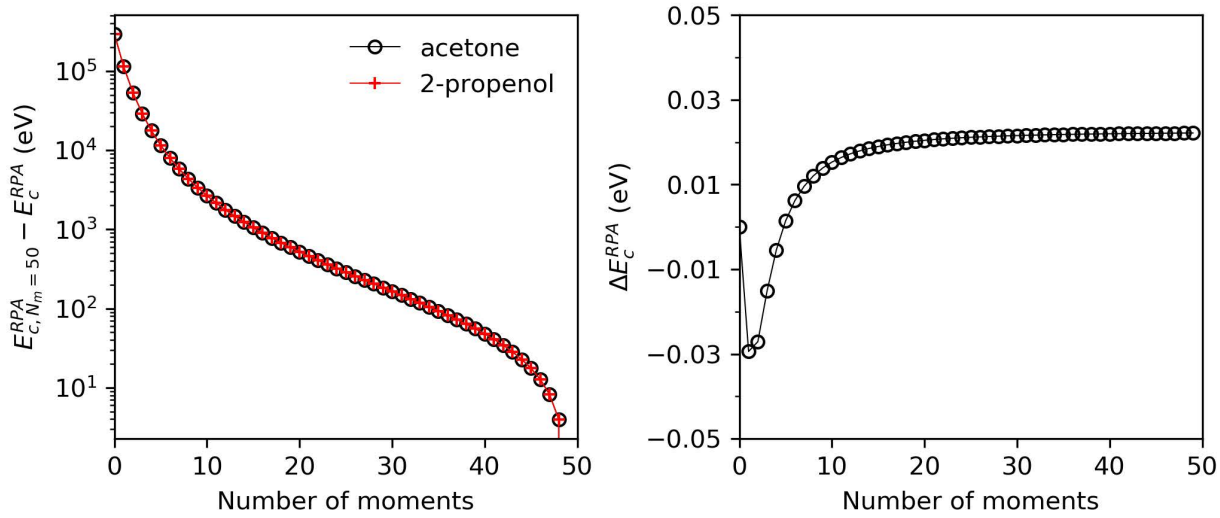

FIG. 2. (a) Convergence of E_c^{RPA} for acetone and 2-propenol with respect the number of moments. E_c^{RPA} is referenced to its value calculated using 50 moments. (b) Convergence of the RPA correlation energy difference. 10000 random vectors are used in these calculations.

for the case of using ACS are similar and are not shown. Therefore, a small number of moments can be used for computing $\Delta E_c^{\mathrm{RPA}}$, which much reduces the computational cost. These observations suggest that RPA-KPM is not very useful for calculating the absolute RPA correlation energies, but is useful for calculating the RPA correlation energy difference between two similar systems.

The convergence of the RPA correlation energy with respect to N_m is related to the convergence of DOS with respect to N_m, which is given in Fig. 3. The results are for $u = 1.03 \times 10^{-5}$ a.u.. Other frequencies give similar observations and are not shown. For both molecules, the first ten eigenvalues are marked by the vertical bars. Both ρ_{acetone} and $\rho_{2-\mathrm{propenol}}$ increase quickly as the eigenvalue approaches zero, due to the fact that most eigenvalues of $v_c^{1/2}\chi_0(iu)v_c^{1/2}$ are close to zero. The resolution of DOSs are determined by N_m. As N_m increases, the peaks associated with these eigenvalues become clear. The convergence of both ρ_{acetone} and $\rho_{2-\mathrm{propenol}}$ is very slow, which explains the slow convergence of their RPA correlation energies observed in Fig. 2(a). In contrast, the convergence of $\Delta\rho$ is much faster, which is the reason for the fast convergence of $\Delta E_c^{\mathrm{RPA}}$ observed in Fig. 2(b).

The performance of ACS is demonstrated in Figure 4(a), which shows the convergence of $\Delta E_c^{\mathrm{RPA}}$ with respect to the number of random vectors. 50 moments are used in the

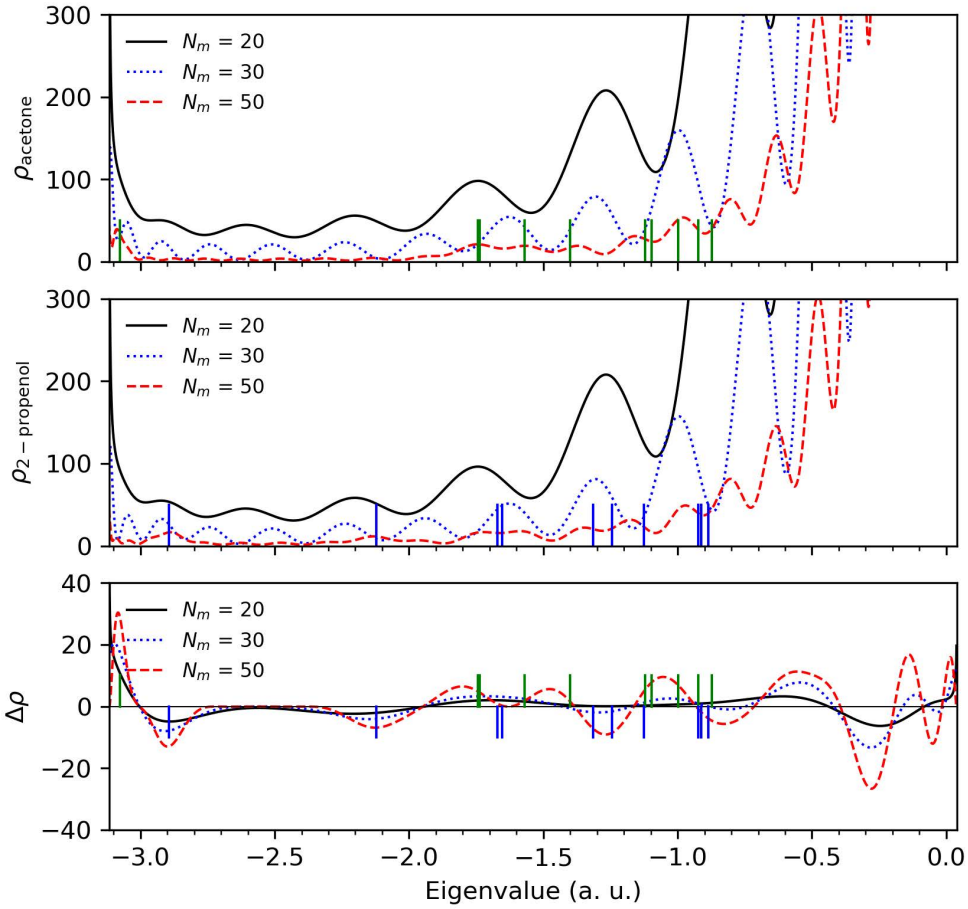

FIG. 3. DOSs of acetone, 2-propenol, and their difference ($\Delta\rho = \rho_{\mathrm{acetone}} - \rho_{2-\mathrm{propenol}}$) calculated using different numbers of moments at $u = 1.03 \times 10^{-5}$ a.u.. The lowest 10 eigenvalues for each molecule are denoted by the vertical bars. In the bottom subplot, acetone and 2-propenol's eigenvalues are marked by the up-pointing green and the down-pointing blue bars, respectively.

calculations. The standard errors are denoted by the red and blue bands. Using ACS, RPA-KPM's results stay closer to the benchmark and have smaller standard errors. The cost reduction due to ACS is 72% (labeled by "All atoms" in Figure 4(b)). This corresponds to an acceleration of 3.6. In other words, for a fixed error in $\Delta E_c^{\mathrm{RPA}}$, the number of random vectors needed by RPA-KPM with using ACS is 3.6 times less than that needed by RPA-KPM without using ACS. To examine each atom's contribution to the cost reduction, we performed ACS for each atom, separately. For instance, the bar labeled by "H1" is obtained by applying ACS only to H1. It is observed that all H atoms do not contribute much to the cost reduction due to their small contribution to the total RPA correlation energy. Most of

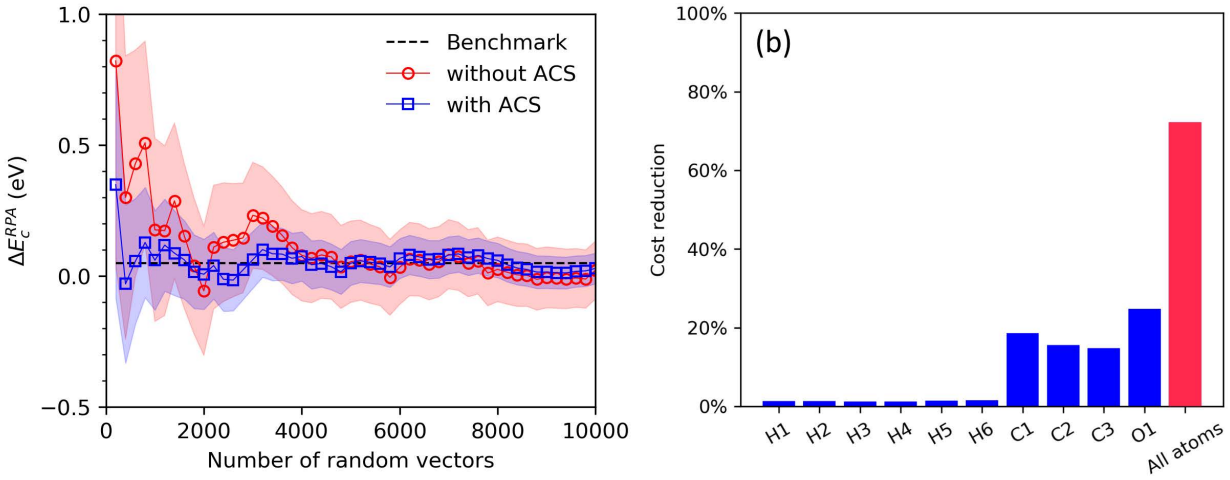

FIG. 4. (a) Convergence of the RPA correlation energy difference between acetone and 2-propenol with respect to the number of random vectors, calculated with and without ACS. Standard errors are represented by the red and blue bands. Benchmark is denoted by the dashed line. (b) Cost reduction for applying ACS to each and to all the atoms. 50 moments are used.

the cost reduction is from C and O atoms. The sum of all atomic cost reduction is 82%, which is larger than the "All atoms" reduction (72%). This is expected because samplings in the atomic regions are not fully decoupled.

B. The water-gas shift reaction

Next, we examine RPA-KPM's performance by calculating the energy of the water-gas shift reaction: $CO + H_2O \rightarrow CO_2 + H_2$. For this example, the system 1 involves two separate RPA-KPM calculations: one for CO and one for H_2O. Similarly, the system 2 involves two separate RPA-KPM calculations: one for CO_2 and one for H_2. The molecules are put in cubic boxes with side length of 10 Å. The RPA part of the reaction energy is obtained as $\Delta E_c^{\mathrm{RPA}} = E_{c,\mathrm{CO}}^{\mathrm{RPA}} + E_{c,\mathrm{H_2O}}^{\mathrm{RPA}} - E_{c,\mathrm{CO_2}}^{\mathrm{RPA}} - E_{c,\mathrm{H_2}}^{\mathrm{RPA}}$, where $E_{c,\mathrm{X}}^{\mathrm{RPA}}$ is the RPA correlation energy of molecule X.

The convergence of $\Delta E_c^{\mathrm{RPA}}$ with respect to the number of random vectors is given in Fig. 5(a). 50 moments are used. Again, as the number of random vectors increases, RPA-KPM results gradually converge to the benchmark. Fig. 5(b) shows the cost reduction by applying ACS to each atom separately, and also by applying ACS to all the atoms. Similar

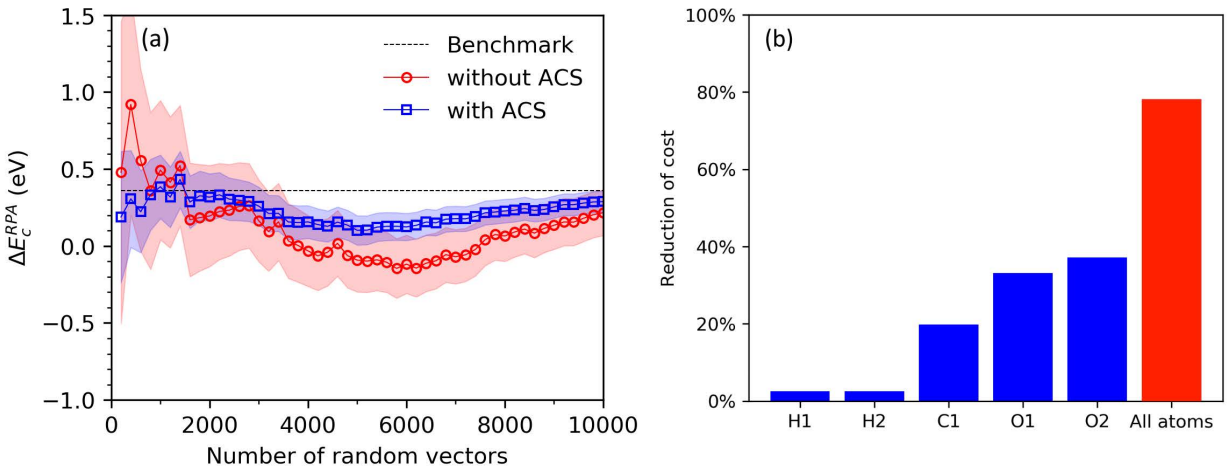

FIG. 5. (a) Convergence of the RPA correlation energy difference between (CO+H_2O) and (CO_2+H_2), with respect to the number of random vectors, calculated with and without ACS. Standard errors are represented by the red and blue bands. Benchmark is denoted by the dashed line. (b) Cost reduction for applying ACS to each atom and to all the atoms. 50 moments are used.

to the above case, the major reductions are from carbon and oxygen, due to their large contribution to the system's RPA correlation energy. By applying ACS to all atoms, the cost is reduced by 78.1%, which gives an acceleration of 4.6 times.

In the above, good convergence of $\Delta E_c^{\mathrm{RPA}}$ with respect to the numbers of random vectors and moments was observed. Here, we verify such convergence by computing the reaction energies of four other reactions: (1) $C_2H_6 + H_2 \rightarrow 2CH_4$, (2) $HCN \rightarrow HNC$, (3) $N_2O + H_2 \rightarrow N_2 + H_2O$, and (4) $N_2 + 3H_2 \rightarrow 2NH_3$. RPA-KPM calculation is performed for each molecule with a kinetic energy cutoff of 300 eV. The molecules are put in 10 Å×10 Å×10 Å boxes. A special attention is paid for the reaction 4, whose energy is calculated as $\Delta E_c^{\mathrm{RPA}} = E_{c,\mathrm{N_2}}^{\mathrm{RPA}} + 3E_{c,\mathrm{H_2}}^{\mathrm{RPA}} - 2E_{c,\mathrm{NH_3}}^{\mathrm{RPA}} - 2E_{c,\mathrm{box}}^{\mathrm{RPA}}$ where $E_{c,\mathrm{box}}^{\mathrm{RPA}}$ is from the RPA-KPM calculation on an empty box. The reason for including $E_{c,\mathrm{box}}^{\mathrm{RPA}}$ is to achieve a good error cancellation. Figure 6 shows $\Delta E_c^{\mathrm{RPA}}$ versus the number of random vectors with 50 moments. The standard errors at 2000 random vectors are similar to the previous two examples. Figure 7 shows that for all reactions $\Delta E_c^{\mathrm{RPA}}$ converges quickly with respect to the number of moments.

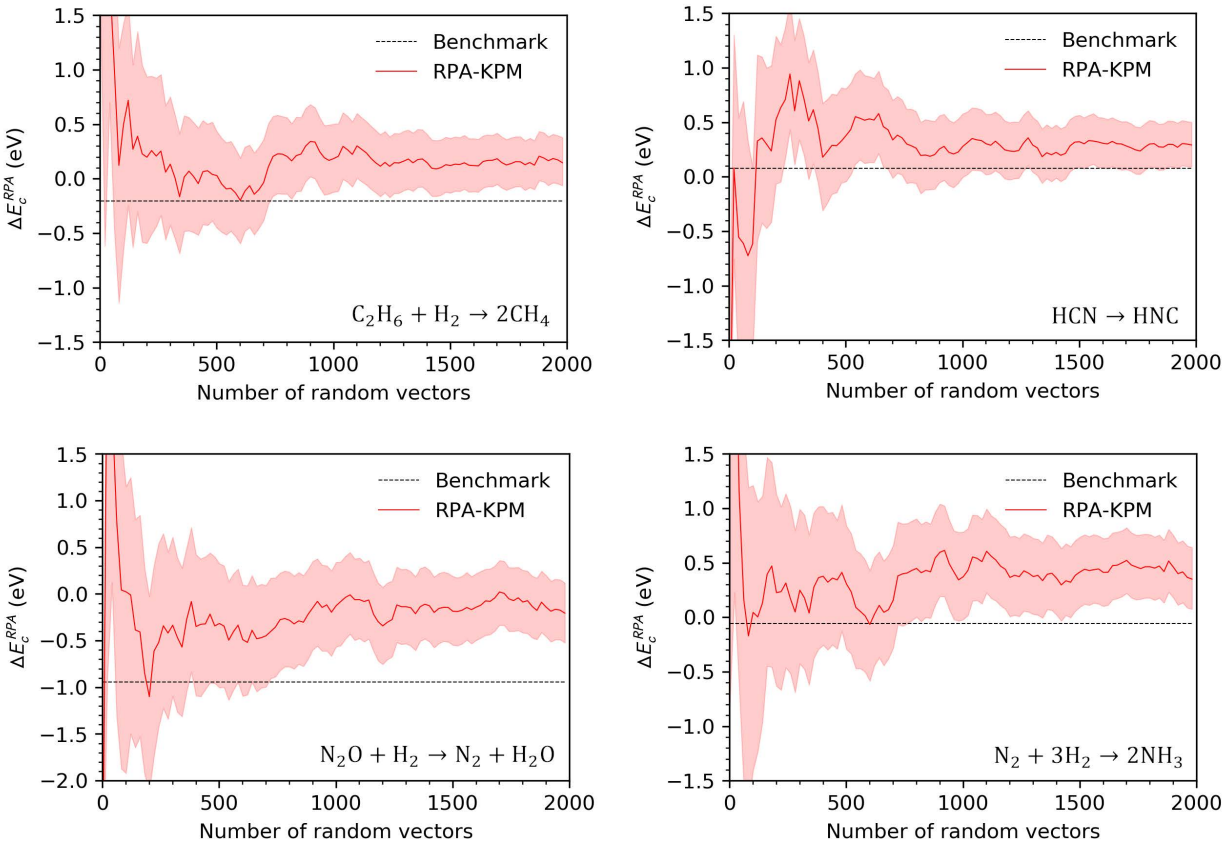

FIG. 6. Convergence of reaction energies with respect to the number of random vectors.

C. H_8 chain

To further understand ACS's performance, we study a simple system: a H_8 chain, in which all atoms are the same. The H-H bond length is 0.7 Å. The system 1 and the system 2 contain the same H_8 chain, and $\Delta E_c^{\mathrm{RPA}}$ equals zero. However, due to the use of two different sequences of random vectors for sampling these two systems, $\Delta E_c^{\mathrm{RPA}}$ is non-zero with a finite number of random vectors.

Fig. 8 shows the cost reduction for different numbers of H atoms used in the ACS scheme. The results are obtained using 2000 random vectors and 30 moments. A good linear relationship between the number of H atoms and the cost reduction is observed. To explain this observation, let's partition the total variance into the variances from the atomic regions and the bond regions. This partitioning assumes that samplings in these two regions are not correlated. This assumption is not true in general, since $v_c^{1/2}\chi_0(iu)v_c^{1/2}$ is not diagonal in real space.

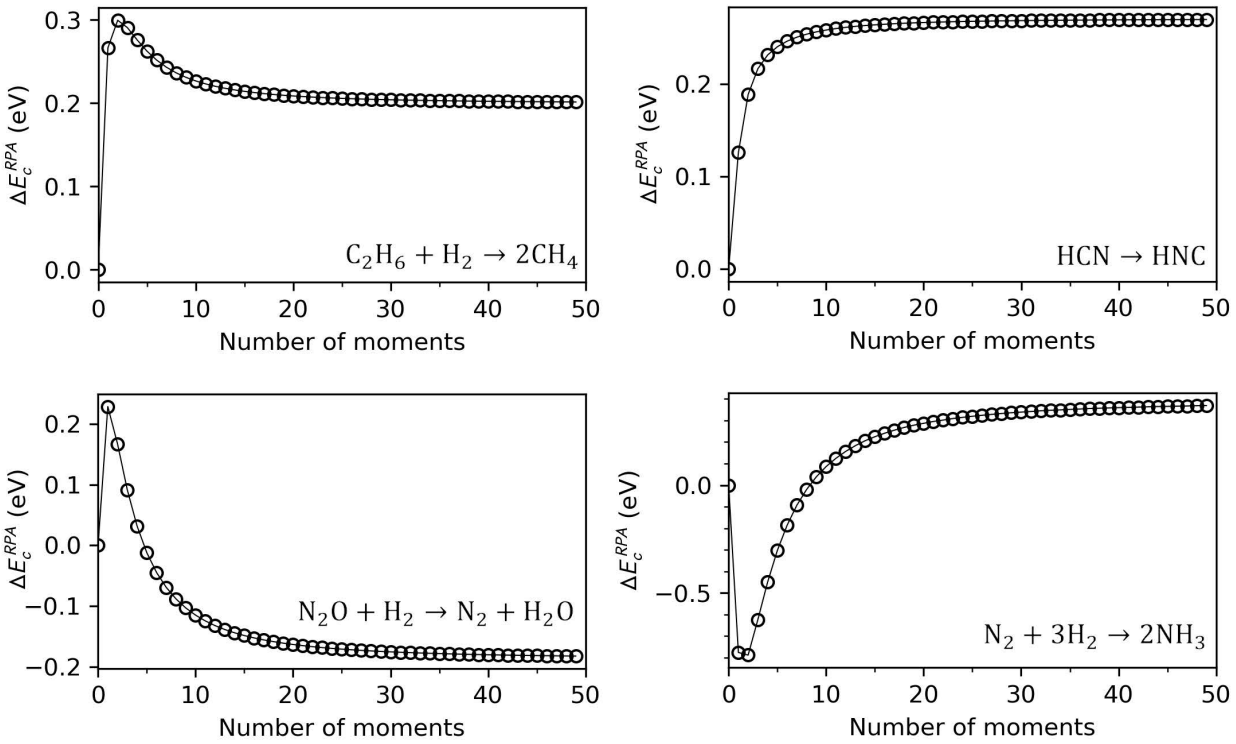

FIG. 7. Convergence of reaction energies with respect to the number of moments.

The H_8 chain has eight H atoms and seven bonds, and Eq. 19 becomes

$$\mathrm{Var}(\Delta E_c^{\mathrm{RPA}}) = 2 \times (8\mathrm{Var}_{\mathrm{atom}} + 7\mathrm{Var}_{\mathrm{bond}}), \tag{22}$$

where $\mathrm{Var}_{\mathrm{atom}}$ and $\mathrm{Var}_{\mathrm{bond}}$ denote the variances from the atomic and bond regions, respectively. By assuming that ACS fully removes the variance from the atomic regions, we obtain the variance for ACS

$$\mathrm{Var}(\Delta E_{c,\mathrm{ACS}}^{\mathrm{RPA}}) = 2 \times ((8-m)\mathrm{Var}_{\mathrm{atom}} + 7\mathrm{Var}_{\mathrm{bond}}), \tag{23}$$

where m is the number of H atoms used in ACS. Following Eq. 21, the cost reduction is a function of m

$$q(m) = 1 - \frac{\mathrm{Var}(\Delta E_{c,\mathrm{ACS}}^{\mathrm{RPA}})}{\mathrm{Var}(\Delta E_c^{\mathrm{RPA}})} = \frac{m\mathrm{Var}_{\mathrm{atom}}}{(8\mathrm{Var}_{\mathrm{atom}} + 7\mathrm{Var}_{\mathrm{bond}})}. \tag{24}$$

By fitting the data in Fig. 8 using $q(m)$, we obtain the ratio $\mathrm{Var}_{\mathrm{atom}}/\mathrm{Var}_{\mathrm{bond}} = 1.5$, which indicates that the variance of the atomic region is about 1.5 times as large as the bond region.

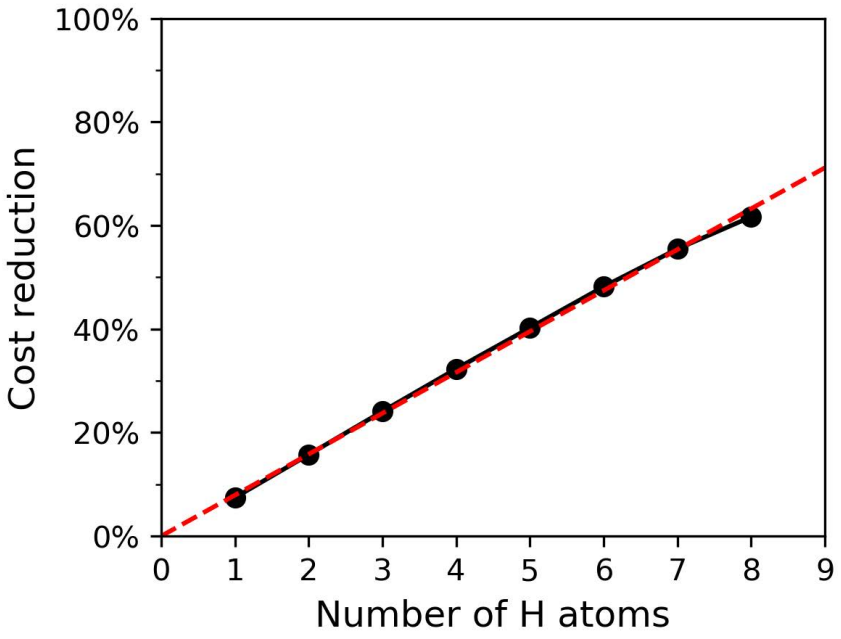

FIG. 8. Cost reduction versus the number of H atoms used in ACS. The red dashed line is obtained by fitting the data with Eq. 24.

D. Computational cost

In this section, we analyze the computational cost of RPA-KPM, and compare it against the stochastic method by Neuhauser and coworkers[26]. The computational parameters that determine their costs are summarized in Table II. See Table II's caption for the meanings of the symbols. First, we discuss RPA-KPM's computational cost, which is estimated as

$$C = N_m N_R N_f C_{step}. \tag{25}$$

N_m, N_R, and N_f are the number of moments, random vectors, and frequencies, respectively. C_{step} is the cost of the dominant step. For RPA-KPM, the dominant step is the calculation of moments using Eq. 12. The calculations rely on computing the perturbed electron density for a perturbing potential, which is obtained by solving the Sternheimer equation whose cost scales as $\mathcal{O}(N_{occ} \times N_{occ} N_g)$. The first factor N_{occ} is due to solving the Sternheimer equation for all occupied states, and the second factor $N_{occ} N_g$ is due to projection to the occupied-state manifold.[51] Thus, we have $C_{step} \sim N_{occ}^2 N_g$. The number of moments is expected to scale with system's size, i.e., $N_m \sim N_g$. To estimate N_R, we note that the sampling error decays as $\sqrt{D/N_R}$ (where $D = N_g$ is the dimension of the $v_c^{1/2} \chi_0(iu) v_c^{1/2}$ matrix)[33]. This gives

TABLE II. Compare RPA-KPM and Neuhauser and coworkers' method[26]. Parameters for calculating both E_c^{RPA} (outside parentheses) and $\Delta E_c^{\mathrm{RPA}}$ (in parentheses) are listed. N_g and N_g are the number of grid points in the system and the region of interest (ROI), respectively. N_{occ} denotes the number of occupied orbitals of the system. N_e and $N_{e,ROI}$ denote the number of electrons in the total system and the region of interest, respectively. N_f is the number of frequencies used for the integration of imaginary frequency iu in Eq. 10. N_R is the number of random vectors.

	RPA-KPM	Method from Ref.[26]
Matrix	$\sqrt{v_c}\chi_0(iu)\sqrt{v_c}$	$\hat{L}$ in Ref.[26]
Dimension of matrix	$N_g \times N_g$	$2N_{occ}N_g \times 2N_{occ}N_g$
Time-consuming step	Linear-response calculation	Apply $\hat{L}$ to a vector
Cost of the time-consuming step	$\sim N_{occ}^2 N_g$	$\sim N_{occ}N_g$
Number of moments	$\sim N_g$ ($\sim N_{g,ROI}$)	$\sim N_{occ}N_g$ ($\sim N_{e,ROI}N_{g,ROI}$)
Number of random vectors	$\sim N_g$ ($\sim N_g \frac{N_{e,ROI}^2}{N_e^2}$)	$\sim N_{occ}N_g$ ($\sim N_{occ}N_g \frac{N_{e,ROI}^2}{N_e^2}$)
Number of frequency	N_f	-
Cost for E_c^{RPA}	$\sim N_{occ}^2 N_g^3 N_f$	$\sim N_{occ}^3 N_g^3$
Cost for $\Delta E_c^{\mathrm{RPA}}$	$\sim N_{occ}^2 N_g^2 N_{g,ROI} \frac{N_{e,ROI}^2}{N_e^2} N_f$	$\sim N_{occ}^2 N_g^2 N_{g,ROI} \frac{N_{e,ROI}^3}{N_e^2}$

$N_R \sim N_g$. Inserting N_m, N_R, and C_{step} into Eq. 25, the total cost C scales as $\mathcal{O}(N_{occ}^2 N_g^3 N_f)$. By assuming N_{occ} and N_g scale with system's size and N_f does not scale with system's size, the cost of RPA-KPM for computing a system's RPA correlation energy scales as the fifth power of that system's size.

Next, we estimate RPA-KPM's cost for calculating $\Delta E_c^{\mathrm{RPA}}$ between two similar systems that only differ much in a local region. The number of moments scales with the number of grid points in the region of interest ($N_{g,ROI}$), that is, $N_m \sim N_{g,ROI}$. The sampling errors of the moments decay as $\sqrt{N_g/N_R}$. The error associated with the electrons inside the region of interest then scales as $\frac{N_{e,ROI}}{N_e}\sqrt{N_g/N_R}$, where N_e and $N_{e,ROI}$ are the numbers of electrons in the system and in the region of interest, respectively. To obtain a fixed error in $\Delta E_c^{\mathrm{RPA}}$, we have $N_R \sim (\frac{N_{e,ROI}}{N_e})^2 N_g$. C_{step} is still due to solving the system's Sternheimer equation, that is, $C_{step} \sim N_{occ}^2 N_g$. With Eq. 25, the cost for calculating $\Delta E_c^{\mathrm{RPA}}$ scales as $\mathcal{O}(N_{occ}^2 N_g^2 N_{g,ROI}(\frac{N_{e,ROI}}{N_e})^2 N_f)$. By assuming that N_{occ}, N_e, and N_g all scale with the system's size and N_f does not depend on the system's size, the cost scales quadratically

with the system's size.

We now compare RPA-KPM with the stochastic method by Neuhauser and coworkers.[26] Our method employs the RPA correlation energy formulated in terms of the density linear response functions (Eq. 1). Their method employed the RPA correlation energy formulated based on the time-dependent Hartree approach.[52–55] The numerical advantages of their method is that their method does not require (a) integrating over the imaginary frequency (which gives $N_f = 1$) or (b) solving the Sternheimer equation. The dominant step in their method is the calculation of the product of $\hat{L}$ (defined in Eq. 4 in Ref.[26]) and a vector. The size of $\hat{L}$ is $2N_{occ}N_g \times 2N_{occ}N_g$, which gives $C_{step} \sim N_{occ}N_g$. This scaling is better than that of solving the Sternheimer equation in our method. The numerical disadvantage of their method is that more moments and random vectors are needed for achieving a fixed error, due to the large size of $\hat{L}$. The number of moments for expanding the DOS of $\hat{L}$ should scale as $N_{occ}N_g$. The sampling error decays as $\sqrt{D'/N_R}$, where $D' = 2N_{occ}N_g$ is the dimension of $\hat{L}$. To achieve the same error as our method, N_R scales as $N_{occ}N_g$. With Eq. 25, the cost for their method scales as $N_{occ}^3 N_g^3$ for computing the total RPA correlation energy. To estimate the cost for calculating $\Delta E_c^{\mathrm{RPA}}$, we note that the number of moments is determined by the size of the region of interest as listed in Table II. The error associated with the electrons in the region of interest decays as $\frac{N_{e,ROI}}{N_e}\sqrt{D'/N_R}$. With $D' \sim N_{occ}N_g$, we have $N_R \sim N_{occ}N_g\frac{N_{e,ROI}^2}{N_e^2}$. Finally, the cost for computing $\Delta E_c^{\mathrm{RPA}}$ scales as $\mathcal{O}(N_{occ}^2 N_g^2 N_{g,ROI}\frac{N_{e,ROI}^3}{N_e^2})$. By assuming that N_{occ}, N_e, and N_g all scale with the system's size, this gives a quadratic scaling (the same as our method).

Last, we estimate the cost for the ACS calculations. ACS's cost is due to the additional RPA-KPM calculations on atoms. The number of occupied orbitals for each atom is on the order of $N_{occ}/N_{\mathrm{atom}}$. The dominant step is solving the atoms' Sternheimer equations, and we have $C_{step} \sim N_{\mathrm{atom}}(N_{occ}/N_{\mathrm{atom}})^2 N_g$. With Eq. 25, ACS's cost then scales as $\mathcal{O}(N_{\mathrm{atom}}(N_{occ}/N_{\mathrm{atom}})^2 N_g N_m N_R N_f)$. Note that N_m, N_f, and N_R used for atomic RPA-KPM calculations are the same as those used for the system's RPA-KPM calculations, that is, $N_m \sim N_{g,ROI}$ and $N_R \sim N_g\frac{N_{e,ROI}^2}{N_e^2}$. Finally, the cost of ACS scales as $\mathcal{O}(N_{\mathrm{atom}}(N_{occ}/N_{\mathrm{atom}})^2 N_g^2 N_{g,ROI}\frac{N_{e,ROI}^2}{N_e^2}N_f)$, which is linear with respect to the system's size (assuming N_{occ}, N_{atom}, N_e, and N_g all scale with the system's size). For large systems, ACS's cost is expected to become negligible compared to the cost of the RPA-KPM calculations on entire systems. For small systems, ACS's cost can be larger than the system's RPA-

KPM calculation. For the acetone isomerization example, the cost for solving all atoms' Sternheimer equations is 13 seconds, which is slightly higher than the cost (10 seconds) for solving acetone and 2-propenol's Sternheimer equations. In practice, ACS's cost can be further reduced if we only need to perform ACS on the atoms in the region of interest. This is possible, if, outside that region, the atoms in the two systems have very similar coordinates. This is often the case for surface catalysis, in which the positions of surface-slab atoms do not change much during the surface reactions.

V. CONCLUSION

In this work, we have developed a kernel polynomial method to calculate the RPA correlation energy. We focused on calculating the RPA correlation energy difference between two systems, which is of much interest in practice. To accelerate the convergence of energy-difference calculations, we have developed a simple, yet effective correlated sampling scheme: atom-based correlated sampling. ACS relies on additional RPA-KPM calculations on atoms, whose calculation cost becomes negligible as the system becomes large. The performance of ACS is examined with two examples: the isomerization of acetone to 2-propenol and the energy of the water-gas shift reaction. The convergences of these two examples are much accelerated by ACS, with a boost factor of 3.6 and 4.5 times, respectively. RPA-KPM and ACS developed in this work would be found useful for calculating reaction energies for the chemical reactions that take place in local regions. One possible application is to calculate the adsorption energies of molecules on transition metal surfaces. Accurate predictions for these adsorption energies are important for predicting the kinetics of heterogeneous catalysis.

VI. ACKNOWLEDGMENTS

This work is supported by the National Science Foundation under CHE-1752769.

---

* chuang3@fsu.edu

[1] P. Hohenberg and W. Kohn, "Inhomogeneous electron gas," Phys. Rev. **136**, B864 (1964).

[2] W. Kohn and L. J Sham, "Self-consistent equations including exchange and correlation effects," Phys. Rev. **140**, A1133 (1965).

[3] J. P. Perdew and A. Zunger, "Self-interaction correction to density-functional approximations for many-electron systems," Physical Review B **23**, 5048–5079 (1981).

[4] P. Mori-Sánchez, A. J. Cohen, and W. Yang, "Self-interaction-free exchange-correlation functional for thermochemistry and kinetics," The Journal of Chemical Physics **124**, 091102 (2006).

[5] A. D. Becke, "A new mixing of hartree–fock and local density-functional theories," The Journal of Chemical Physics **98**, 1372–1377 (1993).

[6] J. Harris and R. O. Jones, "The surface energy of a bounded electron gas," J. Phys. F: Met. Phys. **4**, 1170–1186 (1974).

[7] D. C. Langreth and J. P Perdew, "The exchange-correlation energy of a metallic surface," Solid State Commun. **17**, 1425–1429 (1975).

[8] O. Gunnarsson and B. I. Lundqvist, "Exchange and correlation in atoms, molecules, and solids by the spin-density-functional formalism," Phys. Rev. B **13**, 4274 (1976).

[9] D. C. Langreth and J. P. Perdew, "Exchange-correlation energy of a metallic surface wave-vector analysis," Phys. Rev. B **15**, 2884 (1977).

[10] J. F. Dobson and J. Wang, "Successful test of a seamless van der Waals density functional," Phys. Rev. Lett. **82**, 2123–2126 (1999).

[11] M. Lein, J. F. Dobson, and E. K. U. Gross, "Toward the description of van der waals interactions within density functional theory," J. Comput. Chem. **20**, 12–22 (1999).

[12] F. Furche, "Molecular tests of the random phase approximation to the exchange-correlation energy functional," Phys. Rev. B **64**, 195120 (2001).

[13] M. Fuchs and X. Gonze, "Accurate density functionals: approaches using the adiabatic-connection fluctuation-dissipation theorem," Phys. Rev. B **65**, 235109 (2002).

[14] M. Casadei, X. Ren, P. Rinke, A. Rubio, and M. Scheffler, "Density-functional theory for f-electron systems: The α- γ phase transition in cerium," Phys. Rev. Lett. **109**, 146402 (2012).

[15] L. Schimka, J. Harl, A. Stroppa, A. Grüneis, M. Marsman, F. Mittendorfer, and G. Kresse, "Accurate surface and adsorption energies from many-body perturbation theory," Nature Materials **9**, 741–744 (2010).

[16] G. E. Scuseria, T. M. Henderson, and D. C. Sorensen, "The ground state correlation energy of the random phase approximation from a ring coupled cluster doubles approach," The Journal

of Chemical Physics **129**, 231101 (2008).

[17] J. Harl, L. Schimka, and G. Kresse, "Assessing the quality of the random phase approximation for lattice constants and atomization energies of solids," Phys. Rev. B **81**, 115126 (2010).

[18] H. Eshuis, J. Yarkony, and F. Furche, "Fast computation of molecular random phase approximation correlation energies using resolution of the identity and imaginary frequency integration," J. Chem. Phys. **132**, 234114 (2010).

[19] X. Ren, P. Rinke, V. Blum, J. Wieferink, A. Tkatchenko, A. Sanfilippo, K. Reuter, and M. Scheffler, "Resolution-of-identity approach to hartree–fock, hybrid density functionals, RPA, MP2 andGWwith numeric atom-centered orbital basis functions," New Journal of Physics **14**, 053020 (2012).

[20] M. Kaltak, J. Klimeš, and G. Kresse, "Low scaling algorithms for the random phase approximation: Imaginary time and laplace transformations," Journal of Chemical Theory and Computation **10**, 2498–2507 (2014).

[21] Jan Wilhelm, Patrick Seewald, Mauro Del Ben, and Jürg Hutter, "Large-scale cubic-scaling random phase approximation correlation energy calculations using a gaussian basis," Journal of Chemical Theory and Computation **12**, 5851–5859 (2016).

[22] Mihály Kállay, "Linear-scaling implementation of the direct random-phase approximation," The Journal of Chemical Physics **142**, 204105 (2015).

[23] Shuhua Li, Jing Ma, and Yuansheng Jiang, "Linear scaling local correlation approach for solving the coupled cluster equations of large systems," Journal of Computational Chemistry **23**, 237–244 (2001).

[24] Henry F Schurkus and Christian Ochsenfeld, "Communication: An effective linear-scaling atomic-orbital reformulation of the random-phase approximation using a contracted double-Laplace transformation," J. Chem. Phys. **144**, 031101 (2016).

[25] Arne Luenser, Henry F Schurkus, and Christian Ochsenfeld, "Vanishing-overhead linear-scaling random phase approximation by Cholesky decomposition and an attenuated coulomb-metric," J. Chem. Theory Comput. **13**, 1647–1655 (2017).

[26] D. Neuhauser, E. Rabani, and R. Baer, "Expeditious stochastic calculation of random-phase approximation energies for thousands of electrons in three dimensions," J. Phys. Chem. Lett. **4**, 1172–1176 (2013).

[27] D. Neuhauser, Y. Gao, C. Arntsen, C. Karshenas, E. Rabani, and R. Baer, "Breaking the theoretical scaling limit for predicting quasiparticle energies: The StochasticGWApproach," Physical Review Letters **113** (2014), 10.1103/physrevlett.113.076402.

[28] R. Baer, D. Neuhauser, and E. Rabani, "Self-averaging stochastic kohn-sham density-functional theory," Physical Review Letters **111** (2013), 10.1103/physrevlett.111.106402.

[29] E. Rabani, R. Baer, and D. Neuhauser, "Time-dependent stochastic bethe-salpeter approach," Physical Review B **91** (2015), 10.1103/physrevb.91.235302.

[30] Y. Gao, D. Neuhauser, R. Baer, and E. Rabani, "Sublinear scaling for time-dependent stochastic density functional theory," J. Chem. Phys. **142**, 034106 (2015).

[31] D. Neuhauser, E. Rabani, and R. Baer, "Expeditious stochastic approach for MP2 energies in large electronic systems," J. Chem. Theory Comput. **9**, 24–27 (2012).

[32] R. Baer and D. Neuhauser, "Communication: Monte carlo calculation of the exchange energy," The Journal of Chemical Physics **137**, 051103 (2012).

[33] A. Weiße, G. Wellein, A. Alvermann, and H. Fehske, "The kernel polynomial method," Rev. Mod. Phys. **78**, 275 (2006).

[34] R.N. Silver and H. Röder, "Density of states of mega-dimensional hamiltonian matrices," International Journal of Modern Physics C **05**, 735–753 (1994).

[35] L.-W. Wang, "Calculating the density of states and optical-absorption spectra of large quantum systems by the plane-wave moments method," Physical Review B **49**, 10154–10158 (1994).

[36] L.-W. Wang and A. Zunger, "Dielectric constants of silicon quantum dots," Physical Review Letters **73**, 1039–1042 (1994).

[37] R. N. Silver, H. Roeder, A.F. Voter, and J. D. Kress, "Kernel polynomial approximations for densities of states and spectral functions," Journal of Computational Physics **124**, 115–130 (1996).

[38] Y. M. Niquet, M. Fuchs, and X. Gonze, "Exchange-correlation potentials in the adiabatic connection fluctuation-dissipation framework," Physical Review A **68** (2003), 10.1103/physreva.68.032507.

[39] D. Jackson, Ph.D. thesis, Georg-August-Universitt Gttingen (1911).

[40] D. Jackson, "On approximation by trigonometric sums and polynomials," Trans. Am. Math. Soc. **13**, 491–515 (1912).

[41] R. Piessens, E. de Doncker-Kapenga, C. Überhuber, and D. Kahaner, *Quadpack: A Subroutine Package for AutomaticIntegration* (Springer Series in Computational Mathematics, Springer, New York, 1983).

[42] G. E. P. Box and M. E. Muller, "A note on the generation of random normal deviates," The Annals of Mathematical Statistics **29**, 610–611 (1958).

[43] W. H. Press, S. A. Teukolsky, W. T. Vetterling, and B. P. Flannery, *Numerical Recipes in FORTRAN: The Art of Scientific Computing*, 2nd ed. (Cambridge University Press, Cambridge, UK, 1992).

[44] R. M. Sternheimer, "Electronic polarizabilities of ions from the hartree-fock wave functions," Physical Review **96**, 951–968 (1954).

[45] G. D. Mahan, "Modified sternheimer equation for polarizability," Physical Review A **22**, 1780–1785 (1980).

[46] H.-V. Nguyen and S. de Gironcoli, "Efficient calculation of exact exchange and RPA correlation energies in the adiabatic-connection fluctuation-dissipation theory," Phys. Rev. B **79**, 205114 (2009).

[47] X. Gonze, B. Amadon, P.-M. Anglade, J.-M. Beuken, F. Bottin, P. Boulanger, F. Bruneval, D. Caliste, R. Caracas, M. Côté, T. Deutsch, L. Genovese, Ph. Ghosez, M. Giantomassi, S. Goedecker, D.R. Hamann, P. Hermet, F. Jollet, G. Jomard, S. Leroux, M. Mancini, S. Mazevet, M.J.T. Oliveira, G. Onida, Y. Pouillon, T. Rangel, G.-M. Rignanese, D. Sangalli, R. Shaltaf, M. Torrent, M.J. Verstraete, G. Zerah, and J.W. Zwanziger, "ABINIT: First-principles approach to material and nanosystem properties," Computer Physics Communications **180**, 2582–2615 (2009).

[48] T. Olsen and K. S. Thygesen, "Random phase approximation applied to solids, molecules, and graphene-metal interfaces: From van der Waals to covalent bonding," Phys. Rev. B **87**, 075111 (2013).

[49] J. P. Perdew, K. Burke, and M. Ernzerhof, "Generalized gradient approximation made simple," Phys. Rev. Lett. **77**, 3865 (1996).

[50] K. Momma and F. Izumi, "VESTA3 for three-dimensional visualization of crystal, volumetric and morphology data," J. Appl. Crystallogr. **44**, 1272–1276 (2011).

[51] Stefano Baroni, Stefano De Gironcoli, Andrea Dal Corso, and Paolo Giannozzi, "Phonons and related crystal properties from density-functional perturbation theory," Rev. Mod. Phys. **73**,

515 (2001).

[52] Daniel Neuhauser and Roi Baer, "Efficient linear-response method circumventing the exchange-correlation kernel: Theory for molecular conductance under finite bias," The Journal of Chemical Physics **123**, 204105 (2005).

[53] Filipp Furche, "Developing the random phase approximation into a practical post-kohn–sham correlation model," The Journal of Chemical Physics **129**, 114105 (2008).

[54] Henk Eshuis, Jefferson E. Bates, and Filipp Furche, "Electron correlation methods based on the random phase approximation," Theoretical Chemistry Accounts **131** (2012), 10.1007/s00214-011-1084-8.

[55] Guo P. Chen, Vamsee K. Voora, Matthew M. Agee, Sree Ganesh Balasubramani, and Filipp Furche, "Random-phase approximation methods," Annual Review of Physical Chemistry **68**, 421–445 (2017).